Deterministic entanglement of two trapped ions*

Q. A. Turchette,† C. S. Wood, B. E. King, C. J. Myatt, D. Leibfried,‡ W. M. Itano, C. Monroe, and D. J. Wineland
Time and Frequency Division, National Institute of Standards and Technology, Boulder, CO 80303
(June 4, 1998)

We have prepared the internal states of two trapped ions in both the Bell-like singlet and triplet entangled states. In contrast to all other experiments with entangled states of either massive particles or photons, we do this in a deterministic fashion, producing entangled states *on demand* without selection. The deterministic production of entangled states is a crucial prerequisite for large-scale quantum computation.

Since the seminal discussions of Einstein, Podolsky, and Rosen, two-particle quantum entanglement has been used to magnify and confirm the peculiarities of quantum mechanics [1]. More recently, quantum entanglement has been shown to be not purely of pedagogical interest, but also relevant to computation [2], information transfer [3], cryptography [4] and spectroscopy [5,6]. Quantum computation (QC) exploits the inherent parallelism of quantum superposition and entanglement to perform certain tasks more efficiently than can be achieved classically [7].

Relatively few physical systems are able to approach the severe requirements of QC: controllable coherent interaction between the quantum information carriers (quantum bits or qubits), isolation from the environment, and high-efficiency interrogation of individual qubits. Cirac and Zoller have proposed a *scalable* scheme utilizing trapped ions for QC [8]. In it, the qubits are two internal states of an ion; entanglement and computation are achieved by quantum logic operations on pairs of ions involving shared quantized motion. Previously, quantum logic operations were demonstrated between a single ion's motion and its spin [9]; the requirements of QC have been explored experimentally in related cavity QED systems [10]. In this Letter, we use conditional quantum logic transformations to entangle and manipulate the qubits of two trapped ions.

Previous experiments have studied entangled states of photons [11,12] and of massive particles [13–15]. These experiments rely in some way on *random processes*, either in creation of the entanglement, as in photon cascades [11], photon down-conversion [12] and proton scattering [13], or in the random arrival times of atoms in a cavity [14]. Recent results in NMR of bulk samples have shown entanglement of particle spins [15,16] but because pseudo-pure states are selected through averaging over a thermal distribution, the signal is exponentially degraded as the number of qubits is increased. All the above processes are *selectable* but are not *deterministic* generators of entanglement. By deterministic, we mean that a known and controllable quantum state of (all of) a given set of particles is generated *at a specified time* [17]. Deterministic entanglement coupled with the ability to store entangled states for future use is crucial for the realization of large-scale quantum computation. Ion-trap QC has no fundamental scaling limits; moreover, even the simple two-ion manipulations described here can, in principle, be incorporated into large-scale computing, either by coupling two-ion subsystems via cavities [18], or by using accumulators [6].

In this Letter, we describe the deterministic generation of a state which under ideal conditions is given by

$$|\psi_e(\phi)\rangle = \left[\frac{3}{5}|\downarrow\uparrow\rangle - e^{i\phi}\frac{4}{5}|\uparrow\downarrow\rangle\right] \tag{1}$$

where $|\downarrow\rangle$ and $|\uparrow\rangle$ refer to internal electronic states of each ion (in the usual spin-1/2 analogy) and ϕ is a controllable phase-factor. For $\phi = 0$ or π, $|\psi_e(\phi)\rangle$ is a good approximation to the usual Bell singlet $(-)$ or triplet $(+)$ state $|\psi_B^{\mp}\rangle = [|\downarrow\uparrow\rangle \mp |\uparrow\downarrow\rangle]/\sqrt{2}$ since $|\langle\psi_B^-|\psi_e(0)\rangle|^2 = |\langle\psi_B^+|\psi_e(\pi)\rangle|^2 = 0.98$ [19]. The fidelity of our experimentally generated state described by density matrix $\rho^{\pm}$ is $\langle\psi_e(\pi,0)|\rho^{\pm}|\psi_e(\pi,0)\rangle \approx \langle\psi_B^{\pm}|\rho^{\pm}|\psi_B^{\pm}\rangle \approx 0.70$, so that for all practical purposes, we can consider $\rho^{\pm}$ to be an approximation to the Bell states. We describe a novel means of differentially addressing each ion to generate the entanglement and a state-sensitive detection process to characterize it.

The apparatus is described in Ref. [20]. We confine $^9Be^+$ ions in an elliptical rf Paul trap (major axis $\approx$ 525μm, aspect ratio 3:2) with a potential applied between ring and end-caps of $V_0 \cos\Omega_T t + U_0$ with $\Omega_T/2\pi \approx 238$ MHz, $V_0 \approx 520$ V. The trap is typically operated over the range 12 V $< U_0 <$ 17 V leading to secular frequencies of $(\omega_x, \omega_y, \omega_z)/2\pi = (7.3, 16, 12.6)$ to $(8.2, 17.2, 10.1)$ MHz. The ion-ion spacing (along $\hat{x}$) is $l \approx 2\mu$m.

The relevant level structure of $^9Be^+$ is shown in Fig. 1a. The qubit states are the $2s\ ^2S_{1/2}\ |F = 2, m_F = 2\rangle \equiv |\downarrow\rangle$ and $2s\ ^2S_{1/2}\ |F = 1, m_F = 1\rangle \equiv |\uparrow\rangle$ states. Laser beams D1 and D2 provide Doppler precooling and beam D3 prevents optical pumping to the $|F = 2, m_F = 1\rangle$ state. The cycling $|\downarrow\rangle \rightarrow 2p\ ^2P_{3/2}\ |F = 3, m_F = 3\rangle$ transition driven by the σ^+-polarized D2 laser beam allows us to differentiate $|\uparrow\rangle$ from $|\downarrow\rangle$ in a single ion with $\approx$90% detection efficiency by observing the fluorescence rate.

Transitions $|\downarrow\rangle|n\rangle \leftrightarrow |\uparrow\rangle|n'\rangle$ (where n, n' are vibrational quantum numbers) are driven by stimulated Raman processes from pairs of laser beams in one of two

geometries. Two types of transitions are driven: the "carrier" with $n' = n$, and the red motional sideband (rsb) with $n' = n-1$ [21]. With reference to Fig. 1a, the pair of Raman beams R1 $\perp$ R2 has difference-wavevector $\delta\vec{k} \parallel \hat{x}$ and is used for sideband cooling (to prepare $|\downarrow\downarrow\rangle|0\rangle$), driving the $\hat{x}$-rsb, and to drive the "$\hat{x}$-carrier". Beam pair R2 $\parallel$ R3 has $\delta\vec{k} \approx 0$ and is not sensitive to motion; this pair drives the "co-propagating carrier" transition.

Two trapped ions aligned along $\hat{x}$ have two modes of motion along $\hat{x}$: the center-of-mass (COM) mode at frequency ω_x and the stretch mode, at frequency $\omega_{\rm str} = \sqrt{3}\omega_x$ in which the two ions move in opposite directions. We sideband-cool both of these modes to near the ground state, but use the stretch mode on transitions which involve the motion since it is colder (99% probability of $|n = 0\rangle$) than the COM and heats at a significantly reduced rate [20]. The relevant two-ion qubit level structure dressed by the quantized harmonic stretch motion is shown in Fig. 1b (we leave out the COM for clarity). In general, all four Rabi rates $\Omega_{i\pm}$, $i \in \{1, 2\}$ connecting the levels are different and depend on n. Fig. 1b shows the states coupled on the rsb with Rabi frequencies (in the Lamb-Dicke limit)

$$\Omega_{i+} = \sqrt{n}\,\eta'\Omega_i; \;\; \Omega_{i-} = \sqrt{n+1}\,\eta'\Omega_i \tag{2}$$

where $\eta' = \eta/\sqrt{2\sqrt{3}}$ is the stretch-mode two-ion Lamb-Dicke parameter (with single-ion $\eta \approx 0.23$ for $\omega_x/2\pi \approx$ 8 MHz) and Ω_i is the carrier Rabi frequency of ion i [9]. On the carrier, the ions are not coupled and the time evolution is simply that of independent coherent Rabi oscillations with Rabi frequencies Ω_i. On the co-propagating carrier, $\Omega_1 = \Omega_2 \equiv \Omega_c$.

In the Cirac-Zoller scheme, each of an array of tightly focused laser beams illuminates one and only one ion for individual state preparation. Here we pursue an alternative technique, based not on $\Omega_i \to 0$ for all but one ion, but simply on $\Omega_1 \neq \Omega_2$. Differential Rabi frequencies can be used conveniently for individual addressing on the $\hat{x}$-carrier: for example, if $\Omega_1 = 2\Omega_2$, then ion 1 can be driven for a time $\Omega_1 t = \pi$ (2π-pulse, no spin-flip) while ion 2 is driven for a π-pulse resulting in a spin-flip.

Our technique for differential addressing is to control the ion micro-motion. To a good approximation, we can write

$$\Omega_i = \Omega_c J_0(|\delta\vec{k}|\xi_i) \tag{3}$$

where J_0 is the zero-order Bessel function and ξ_i is the amplitude of micro-motion (along $\hat{x}$) associated with ion i, proportional to the ion's mean displacement from trap center. The micro-motion is controlled by applying a static electric field to push the ions [22] along $\hat{x}$, moving ion 2 (ion 1) away from (toward) the rf null position, inducing a smaller (larger) Rabi frequency. The range of Rabi frequencies explored experimentally is shown in Fig. 2a.

We determine $\Omega_{1,2}$ by observing the Rabi oscillations of the ions driven on the $\hat{x}$-carrier. An example with $\Omega_1 = 2\Omega_2$ is shown in Fig. 2b. We detect a fluorescence signal $S(t) = 2P_{\downarrow\downarrow} + (1+\alpha)P_{\downarrow\uparrow} + (1-\alpha)P_{\uparrow\downarrow}$ where $P_{kl} = |\langle\psi(t)|kl\rangle|^2$, $k, l \in \{\uparrow, \downarrow\}$, $\psi(t)$ is the state at time t and $|\alpha| \ll 1$ describes a small differential detection efficiency due to the induced differential micro-motion. Driving on the $\hat{x}$-carrier for time t starting from $|\downarrow\downarrow\rangle|0\rangle$, $S(t)$ can be described by

$$\begin{aligned} S(t) = 1 &+ (1/2)(1+\alpha)\cos(2\Omega_1 t)e^{-\gamma t} \\ &+ (1/2)(1-\alpha)\cos(2\Omega_2 t)e^{-(\Omega_2/\Omega_1)\gamma t} \end{aligned} \tag{4}$$

where γ allows for decay of the signal [21]. The local maximum at $t = 2.4$ μs on Fig. 2b is the $2\pi : \pi$ point at which ion 1 has undergone a 2π-pulse while ion 2 has undergone a π-pulse resulting in $|\downarrow\downarrow\rangle|0\rangle \to |\downarrow\uparrow\rangle|0\rangle$. Driving a $\pi : \pi$ pulse on the co-propagating carrier transforms $|\downarrow\uparrow\rangle|0\rangle$ to $|\uparrow\downarrow\rangle|0\rangle$ and $|\downarrow\downarrow\rangle|0\rangle$ to $|\uparrow\uparrow\rangle|0\rangle$, completing generation of all four internal basis states of Fig. 1b.

Now consider the levels coupled by the first rsb shown in Fig. 1b. If we start in the state $|\psi(0)\rangle = |\downarrow\uparrow\rangle|0\rangle$ and drive on the (stretch mode) rsb for time t,

$$\begin{aligned} |\psi(t)\rangle = &-\frac{i\Omega_{2-}}{G}\sin(Gt)|\downarrow\downarrow\rangle|1\rangle \\ &+ \left[\frac{\Omega_{2-}^2}{G^2}(\cos Gt - 1) + 1\right]|\downarrow\uparrow\rangle|0\rangle \\ &+ e^{i\phi}\left[\frac{\Omega_{2-}\Omega_{1-}}{G^2}(\cos Gt - 1)\right]|\uparrow\downarrow\rangle|0\rangle \end{aligned} \tag{5}$$

where $G = (\Omega_{2-}^2 + \Omega_{1-}^2)^{1/2}$ with Ω_{i-} from Eq. 2 with $n = 0$. The phase factor $\phi = \delta\vec{k} \cdot \langle\vec{x}_1 - \vec{x}_2\rangle$ depends on the spatial separation of the ions and arises because each ion sees a different phase in the $\hat{x}$ travelling-wave Raman field. The ion-ion spacing varies by $\delta l \approx 100$ nm over the range of U_0 cited above ($\phi = 0$ for $U_0 = 16.3$ V and $\phi = \pi$ for $U_0 = 12.6$ V, with $d\phi/dU_0$ in good agreement with theory). For $Gt = \pi$, the final state is $\psi_e(\phi)$ from Eq. 1. Note that $\Omega_1 = (\sqrt{2}+1)\Omega_2$ would generate the Bell states (but we would not have access to the initial state $|\downarrow\uparrow\rangle$, since Ω_i are fixed throughout an experiment).

We now describe our two-ion state-detection procedure. We first prepare a two-ion basis state $|kl\rangle$, apply the detection beam D2 for a time $\tau_d \approx 500\mu$s and record the number of photons m detected in time τ_d. We repeat this sequence for $N \approx 10^4$ trials and build a histogram of the photons collected (Fig. 3). To determine the populations of an unknown state, we fit its histogram to a weighted sum of the four reference histograms with a simple linear least-squares procedure.

We observe that the $|\uparrow\uparrow\rangle$ count distribution (Fig. 3a) is not a single peak at $m = 0$, corresponding to the expected zero scattered photons. Counts at $m = 1$ and $m = 2$ are due to a background of 200-400 photons per second. The counts in bins $m > 2$ (which account for $\sim 10\%$ of the area) are due to a depumping process in which D2 off-resonantly drives an ion out of $|\uparrow\rangle$ ultimately trapping it in the cycling transition.

We approximately double the depumping time by applying two additional Raman "shelving" pulses ($|\uparrow\rangle \rightarrow {}^2S_{1/2}|F=2, m_F=0\rangle \rightarrow {}^2S_{1/2}|F=1, m_F=-1\rangle$; $|\downarrow\rangle$ unaffected) after every state preparation. Nevertheless, this results in an average difference of only 10-15 detected photons between an initial $|\downarrow\rangle$ and $|\uparrow\rangle$ state, as shown in Fig. 3 [23]. The distributions associated with $|\downarrow\uparrow\rangle$,$|\uparrow\downarrow\rangle$ and $|\downarrow\downarrow\rangle$ are non-Poissonian due to detection laser intensity and frequency fluctuations, the depumping described above and $|\downarrow\rangle \rightarrow |\uparrow\rangle$ transitions from imperfect polarization of D2.

One may ask: what is our overall two-ion state-detection efficiency on a *per experiment* basis? To address this issue, we distinguish three cases: 1) $|\uparrow\uparrow\rangle$, 2) $|\uparrow\downarrow\rangle$ or $|\downarrow\uparrow\rangle$, 3) $|\downarrow\downarrow\rangle$. Now define case 1 to be true when $m \leq 3$, case 2 when $3 < m < 17$, and case 3 when $m \geq 17$. This gives an optimal 80% probability that the inferred case (1, 2, or 3) from a measured m in a single experiment is the actual case.

We have generated states described by density operators $\rho^{\pm}$ in which the populations (diagonals of $\rho^{\pm}$) are measured to be $P_{\downarrow\uparrow} \approx P_{\uparrow\downarrow} \approx 0.4$, $P_{\downarrow\downarrow} \approx 0.15$, $P_{\uparrow\uparrow} \approx 0.05$. To establish coherence, consider first the Bell singlet state ψ_B^- which has $P_{\downarrow\uparrow} = P_{\uparrow\downarrow} = 1/2$. Since ψ_B^- has total spin $J = 0$, any J-preserving transformation, such as an an equal rotation on both spins, must leave this state unchanged, whereas such a rotation on a mixed state with populations $P_{\downarrow\uparrow} = P_{\uparrow\downarrow} = 1/2$ and no coherences will evolve quite differently. We rotate both spins trough an angle θ by driving on the co-propagating carrier for a time t such that $\theta = \Omega_c t$. Fig. 4a shows the time evolution of an experimental state which approximates the singlet Bell state. Contrast this with the approximate "triplet" state shown in Fig. 4b. More quantitatively, the data show that $\rho^{\pm}$ is decomposed as $\rho^{\pm} = C|\psi_B^{\pm}\rangle\langle\psi_B^{\pm}| + (1-C)\rho_m$ in which ρ_m has no coherences which contribute to the measured signal (off diagonal elements connecting $|\uparrow\downarrow\rangle$ with $|\downarrow\uparrow\rangle$ and $|\uparrow\uparrow\rangle$ with $|\downarrow\downarrow\rangle$), and $C = 0.6$ is the contrast of the curves in Fig. 4. This leads to a fidelity of $\langle\psi_B^{\pm}|\rho^{\pm}|\psi_B^{\pm}\rangle = (P_{\downarrow\uparrow} + P_{\uparrow\downarrow} + C)/2 \approx 0.7$.

The non-unit fidelity of our states arises from several technical factors. The first is Raman laser intensity noise which gives rise to a noise-modulated Rabi-frequency. The second is a second-order (in η) effect on Ω_i due to the motional state of the COM mode [6], which is not in the ground state at all times [20]. These effects can be seen in Fig. 2b as a decay envelope on the data (modeled by γ of Eq. 4) and cause a 10% infidelity in initial state preparation [24]. This initial imperfection in state preparation, the contribution of the above factors on the rsb pulse and a first order effect due to imperfect ground-state preparation of the stretch mode are responsible for the rest of the infidelity.

The micro-motion-induced selection of Rabi frequencies as here demonstrated is sufficient to implement universal quantum logic with individual addressing [8]. To isolate ion 1, we arrange the trap strength and static electric field so that ion 1 is at the rf null position ($\Omega_1 = \Omega_c J_0(0) = \Omega_c$) and ion 2 is at a position such that $\Omega_2 = \Omega_c J_0(|\delta\vec{k}|\xi_2) = 0$. To isolate ion 2, we drive on the first motional sideband of the rf-micro-motion by adding $\Omega_T/2\pi = \pm 238$ MHz to the difference frequency of the Raman beams resulting in $\Omega_1 = \Omega_c J_1(0) = 0$ and $\Omega_2 = \Omega_c J_1(|\delta\vec{k}|\xi_2) = 0.519\Omega_c$. This provides a means of individual addressing, with which the Cirac-Zoller scheme [8] can be implemented for two ions.

In conclusion, we have taken a first step in the quantum preparation and manipulation of entangled states of multiple trapped ions— a step which is crucial for quantum computations with trapped ions. We have *engineered* entangled states deterministically, that is, there is no inherent probabilistic nature to our quantum entangling source. We have developed a two-ion state-sensitive detection technique which allows us to measure the diagonal elements of the density matrix $\rho^{\pm}$ of our states, and have performed transformations which directly measure the relevant off-diagonal coherences of $\rho^{\pm}$.

We acknowledge support from the U. S. National Security Agency, Office of Naval Research and Army Research Office. We thank Eric Cornell, Tom Heavnor, David Kielpinski, and Matt Young for critical readings of the manuscript.

---

* Work of the US government. Not subject to US copyright.
† quentint@boulder.nist.gov.
‡ Present address: Institut für Experimentalphysik, Univ. Innsbruck, Austria.

[1] A. Einstein, B. Podolsky, and N. Rosen, Phys. Rev. **47**, 777 (1935). J. S. Bell, *Speakable and unspeakable in quantum mechanics* (Cambridge University Press, Cambridge, England, 1987).
[2] P. W. Shor, SIAM J. Comp. **26**, 1484 (1997). L. K. Grover, Phys. Rev. Lett. **79**, 325 (1997).
[3] A. Barenco and A. Ekert, J. Mod. Opt. **42**, 1253 (1995). C. H. Bennett, Phys. Today **48**, 24 (Oct., 1995);
[4] A. Ekert, Phys. Rev. Lett. **67**, 661 (1991). C. H. Bennett, Sci. Am. **267**, 50 (Oct., 1992).
[5] J. J. Bollinger *et al.*, Phys. Rev. **A54**, R4649 (1996); S. F. Huelga *et al.*, Phys. Rev. Lett. **79**, 3865 (1997).
[6] D. W. Wineland *et al.*, to appear in NIST Journal of Research; e-print at quant-ph/9803023 (unpublished).
[7] A. Ekert and R. Jozsa, Rev. Mod. Phys. **68**, 733 (1996). A. Steane, Rep. Prog. Phys. **61**, 117 (1998).
[8] J. I. Cirac and P. Zoller, Phys. Rev. Lett. **74**, 4091 (1995).
[9] C. Monroe *et al.*, Phys. Rev. Lett. **75**, 4714 (1995).
[10] Q. A. Turchette *et al.*, Phys. Rev. Lett. **75**, 4710 (1995), X. Maitre *et al.*, Phys. Rev. Lett. **79**, 769 (1997).
[11] S. J. Freedman and J. F. Clauser, Phys. Rev. Lett. **28**, 938 (1972). E. S. Fry and R. C. Thompson, Phys. Rev.

Lett. **37**, 465 (1976). A. Aspect, P. Grangier, and G. Roger, Phys. Rev. Lett. **49**, 91 (1982).

[12] Y. H. Shih and C. O. Alley, Phys. Rev. Lett. **68**, 3663 (1992). Z. Y. Ou and L. Mandel, Phys. Rev. Lett. **61**, 50 (1988). Z. Y. Ou *et al.*, Phys. Rev. Lett. **68**, 3663 (1992). P. Kwiat *et al.*, Phys. Rev. Lett. **75**, 4337 (1995). W. Tittel *et al.*, Europhys. Lett. **40**, 595 (1997). D. Bouwmeester *et al.*, Nature **390**, 575 (1997).

[13] M. Lamehi-Rachti and W. Mittig, Phys. Rev. D **14**, 2543 (1976).

[14] E. Hagley *et al.*, Phys. Rev. Lett. **79**, 1 (1997).

[15] R. Laflamme *et al.*, e-print at quant-ph/9709025 (unpublished).

[16] I. L. Chuang, N. Gershenfeld, and M. Kubinec, Phys. Rev. Lett. **80**, 3408 (1998). I. L. Chuang *et al.*, e-print at quant-ph/9801037 (unpublished). D. G. Corey, M. D. Price, and T. F. Havel, e-print at quant-ph/9709001 (unpublished). D. G. Corey *et al.*, e-print at quant-ph/9802018 (unpublished).

[17] C. K. Law and H. J. Kimble, J. Mod. Opt. **44**, 2067 (1997).

[18] J. I. Cirac *et al.*, Phys. Rev. Lett. **78**, 3221 (1997).

[19] Note that $E(\psi_e(\phi)) = 0.94$ where E is the *entanglement* defined in C. H. Bennett *et al.* , Phys. Rev. A **53**, 2046 (1996).

[20] B. E. King *et al.*, submitted; e-print at quant-ph/9803023.

[21] D. M. Meekhof *et al.*, Phys. Rev. Lett. **76**, 1796 (1996); **77**, 2346 (1996)

[22] S. R. Jefferts *et al.*, Phys. Rev. **A51**, 3112 (1995).

[23] This off-resonant de-pumping can be suppressed by increasing the energy separation between $|\downarrow\rangle$ and $|\uparrow\rangle$ with a strong magnetic field or by using a heavier ion with larger hyperfine splitting.

[24] The reference histograms for $|\downarrow\uparrow\rangle$ and $|\uparrow\downarrow\rangle$ (Figs. 3b,c) have had this 10% contamination from $|\uparrow\uparrow\rangle$ and $|\downarrow\downarrow\rangle$ removed, in order to assure that the references to which we fit are accurate representations of the underlying states.

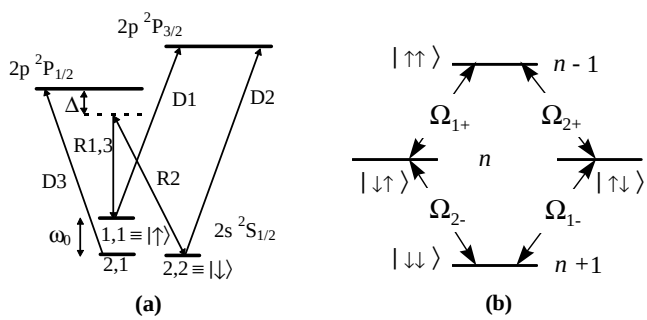

FIG. 1. (a) Relevant $^9Be^+$ energy levels. All optical transitions are near $\lambda = 313$ nm, $\Delta/2\pi = 40$ GHz and $\omega_0/2\pi = 1.25$ GHz. R1-3: Raman beams. D1-3: Doppler cooling, optical pumping and detection beams. (b) The internal basis qubit states of two spins shown with the vibrational levels connected on the red motional sideband. The labeled atomic states are as in (a); n is the motional-state quantum number (note that the motional mode frequency $\omega_{\rm str} \ll \omega_0$). $\Omega_{i\pm}$ are the Rabi frequencies connecting the states indicated.

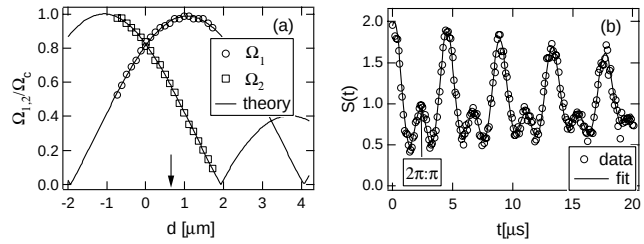

FIG. 2. (a) Normalized $\hat{x}$-carrier Rabi frequencies Ω_i/Ω_c of each of two ions as a function of center-of-mass displacement from the rf-null position d. The solid curves are Eq. 3 where the distance between the maxima of the two curves sets the scale of the ordinate, based on the known ion-ion spacing of $l \approx 2.2\mu$m at $\omega_x/2\pi = 8.8$ MHz. (b) Example of Rabi oscillations with $\Omega_1 = 2\Omega_2$. A fit to Eq. 4 determines that $\Omega_1/2\pi = 2\Omega_2/2\pi \approx 225$ kHz, $\gamma/2\pi \approx 6$ kHz and $\alpha \approx -0.05$. The arrow in (a) indicates the conditions of (b).

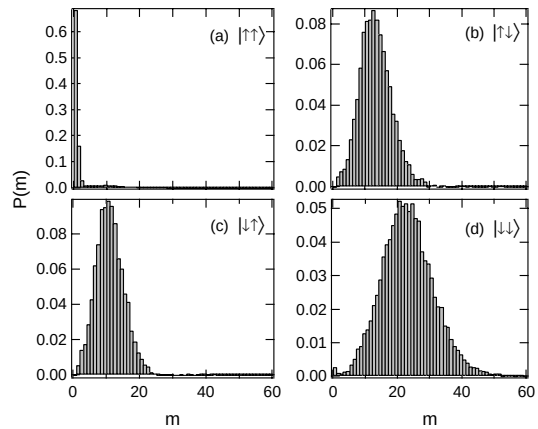

FIG. 3. Photon-number distributions for the four basis qubit states. Plotted in each graph is the probability of occurrence $P(m)$ of m photons detected in 500 μs *vs.* m, taken over $\sim 10^4$ trials. Note the different scales for each graph.

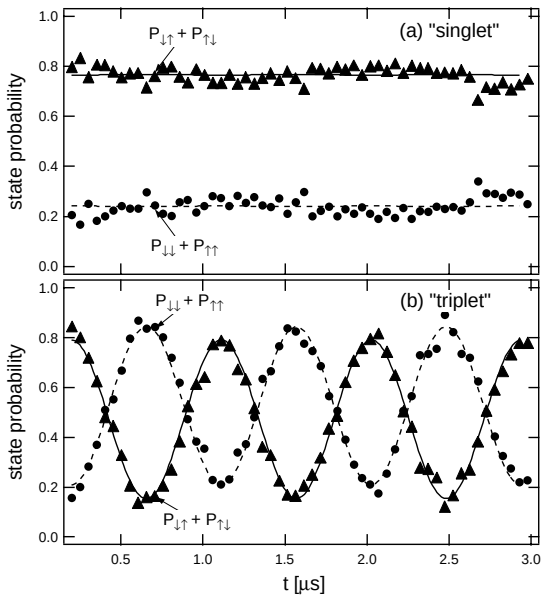

FIG. 4. Probabilities $P_{\downarrow\uparrow} + P_{\uparrow\downarrow}$ and $P_{\downarrow\downarrow} + P_{\uparrow\uparrow}$ as a function of time t driving on the co-propagating carrier, starting from (a) the "singlet" $\psi_e(0)$ and (b) the "triplet" $\psi_e(\pi)$ entangled states. The equivalent rotation angle is $2\Omega_c t$ ($\Omega_c/2\pi \approx 200$ kHz for these data). The solid and dashed lines in (a) and (b) are sinusoidal fits to the data, from which the contrast is extracted.